substance: $PtSb_2$
property: transport properties

See also document .

electrical resistivity

(Figs. 2...5, see also Fig. 1 and 22)

ρ_i	1 Ω cm	T = 70 K	intrinsic value	68R,
	0.1 Ω cm	T = 90 K		83D
	0.01 Ω cm	T = 135 K		
	0.001 Ω cm	T = 250 K		

Hall coefficients
(Figs. 5...8)

R_H	+ 4 cm^3 C^{-1}	T = 2...120 K, B < 3 T	single crystal, intrinsic near RT	73A
	+ 3.0 cm^3 C^{-1}	T = 77...120 K, B < 1.1 T	Te doped single crystal with ρ = 0.0035 Ω cm at 77 K	65D
	+ 103 cm^3 C^{-1}	T = 77 K	single crystal with ρ = 0.0176 Ω cm at 77 K	83D
	– 110 cm^3 C^{-1}	T = 77 K	single crystal with ρ = 0.58 Ω cm at 77 K	68R
	– 600 cm^3 C^{-1}	T = 62.5 K		

thermoelectric powers
(Figs. 9 and 10)

S	+ 80 μV K^{-1}	T = 300 K	polycrystalline sample	63H
	+ 180 μV K^{-1}	T = 80 K	pure and Au doped (n-type $PtSb_2$ by doping with Te)	65J
	– 200 μV K^{-1}		Te doped single crystal with	83D
	– 825 μV K^{-1}	T = 25 K	donor excess n_d–n_a ≈ 10^{17} cm^{-3}	
	0 μV K^{-1}	T = 100 K	and n_a/n_d ≈ 0.8; ΔT ≤ 0.2 K	
	+ 150 μV K^{-1}	T = 125 K		

mobility of charge carriers
(in cm^2/V s)

μ_n	420	T = 300 K	from $\rho(T)$ and $R_H(T)$ in the mixed-conduction range; $\mu_n = 2.07 \cdot 10^6\ T^{-3/2} \exp(12.6\ K/T)$	68R
	3700	T = 77 K		
	2100	T = 50 K	maximum of $R_H\sigma$	68E
	$3 \cdot 10^6\ T^{-3/2}$	T = 7...50 K	acoustic-phonon-limited mobility, from $\rho(T)$ and $R_H(T)$	83D
μ_p	830	T = 300 K	$\mu_n = 4.15 \cdot 10^6\ T^{-3/2} \exp(12.6\ K/T)$	68R
	7300	T = 77 K	$\approx 6.55 \cdot 10^6\ T^{-1.57}$ above 100 K	
	$7.5 \cdot 10^6\ T^{-3/2}$	T = 7...50 K		83D

temperature dependence: Figs. 11...13

In the impurity-conduction range the mobility is temperature independent which suggests that a metallic rather than a hopping type of impurity conduction is dominant [68R]. Between 10 and 40 K the mobilities are limited primarily by ionized-impurity scattering [68R]. The occurrence of the near $T^{-3/2}$ dependence of μ_n and μ_p over a wide temperature range shows that acoustic-mode lattice scattering limits the free-carrier mobilities in sufficiently pure $PtSb_2$ [68R, 68E]. Better agreement with experimental data by taking into account scattering by ionized impurities at low T and by optical phonons at higher T [83D]. Hole and electron mobility are independent of the electric field up to the impact ionization threshold, 1 and 3 kV cm^{-1}, respectively [80D].

mobility ratio
(Fig. 11)

b	0.57	$T \approx 110$ K	from $R_H^{max}/R_H^{exh} = (1-b)^2/4b$, taking R_H^{max} at 110 K and R_H^{exh} in the exhaustion region at 74 K	68E
	0.5	T = 78...200 K	same procedure as above. Te doped single crystals with $n_d - n_a = 0.3...3.2 \cdot 10^{16}$ cm^{-3}	76A
	0.47...0.52	T = 80...300 K	from R_H in the acoustic phonon scattering region of different samples	68R
	0.4	T = 240 K	from $R_H(T)$and $S(T)$	73A
	1	T = 560 K	sign change of $R_H(T)$	
	0.4	T = 10...100 K	acoustic phonon scattering only; total b increases with T	83D

intrinsic carrier concentration

n_i	$7.7 \cdot 10^{18}$ cm^{-3}	T = 300 K	calculated from the experimental value of ρ_i and the equations given above for μ_n and μ_p	68R
	$2.2 \cdot 10^{15}$ cm^{-3}	T = 77 K	calculated as $n_i = 2.72\ A \exp(-0.11\ \text{eV}/2kT)$ with $A = 4.84 \cdot 10^{15}\ T^{3/2}$ [$K^{-3/2}$ cm^{-3}]	
	$1.3 \cdot 10^{16}\ T^{3/2}$ exp $(-640/T)$ [cm^{-3}]	> 100 K	from $\rho(T)$ and $R_H(T)$ using a single parabolic conduction and valence band model	83D

For temperature dependence of $n_i/T^{3/2}$, see Figs. 14 and 15.

magnetoresistance in p-type crystals of low carrier concentration: Fig. 16.

oscillatory magnetoresistance in crystals of high carrier concentration: Figs. 17...19.

dependence of the **resistivity** on hydrostatic pressure: Fig. 20.

piezoresistance coefficients in the range 80...300 K: Fig. 21.

References:

63H Hulliger, F.: Nature (London) 200 (1963) 1064.
65D Damon, D. H., Miller, R. C., Sagar, A.: Phys. Rev. A 138 (1965) 636.
65J Johnston, W. D., Miller, R. C., Damon, D. H.: J. Less-Common Met. 8 (1965) 272.
66B Bennett, S. L., Heyding, R. D.: Can. J. Chem. 44 (1966) 3017.
68E Elliott, C. T., Hiscocks, S. E. R.: J. Mater. Sci. 3 (1968) 174.
68R Reynolds, R. A., Brau, M. J., Chapman, R. A.: J. Phys. Chem. Solids 29 (1968) 755.
72D Damon, D. H., Miller, R. C., Emtage, P. R.: Phys. Rev. B5 (1972) 2175.
73A Abdullaev, A. A., Angelova, L. A., Kuznetsov, V. K., Ormont, A. B., Pashintsev, Yu. I.: Phys. Status Solidi (a) 18 (1973) 459.
76A Alekseeva, V. G., Kuznetsov, V. K., Morenkov, A. D.: Fiz. Tekh. Poluprovodn. 10 (1976) 458; translation: Sov. Phys. Semicond. 10 (1976) 274.
77K Kjekshus, A., Rakke, T.: Acta Chem. Scand. A31 (1977) 517.
80D Dargys, A., Kundrotas, J.: Phys. Status Solidi (b) 100 (1980) K9.
82K Kundrotas, J., Dargys, A.: Litov. Fiz. Sb. 22 (1982) 74.
83D Dargys, A., Kundrotas, J.: J. Phys. Chem. Solids 44 (1983) 261.

Fig. 1.

PtP_2, $PtAs_2$, $PtSb_2$, $PtBi_2$. Resistivity vs. reciprocal temperature [65J]. The data for semimetallic pyrite-typ $PtBi_2$ (h) are added for comparison. PtP_2: hot-pressed sample; $PtAs_2$ and $PtBi_2$: sintered samples; $PtSb_2$: open triangles - polycrystalline sample, full triangles - single crystals. The broken curve shows the measurements of [66B] on a sintered $PtAs_2$ sample.

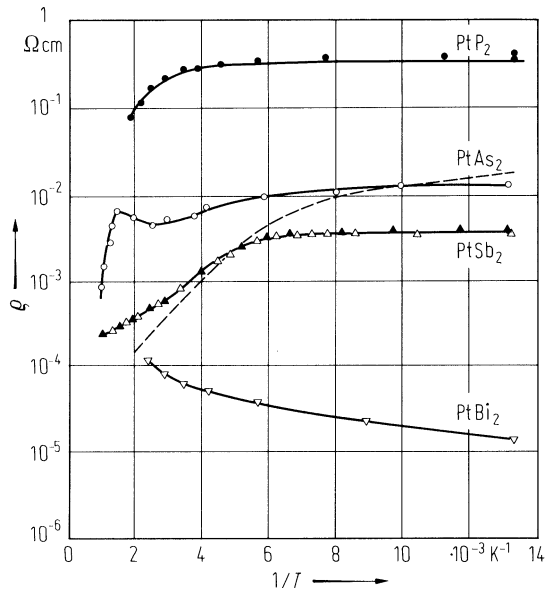

Fig. 2.

$PtSb_2$. Conductivity vs. reciprocal temperature [65D]. Single crystal specimens as in Fig. 6.

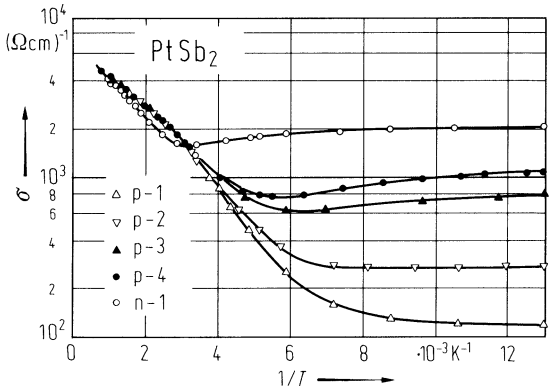

Fig. 3.

$PtSb_2$. Resistivities vs. reciprocal temperature for n-type samples [68R]. Carrier concentrations given in Fig. 7. ρ_i: intrinsic resistivity.

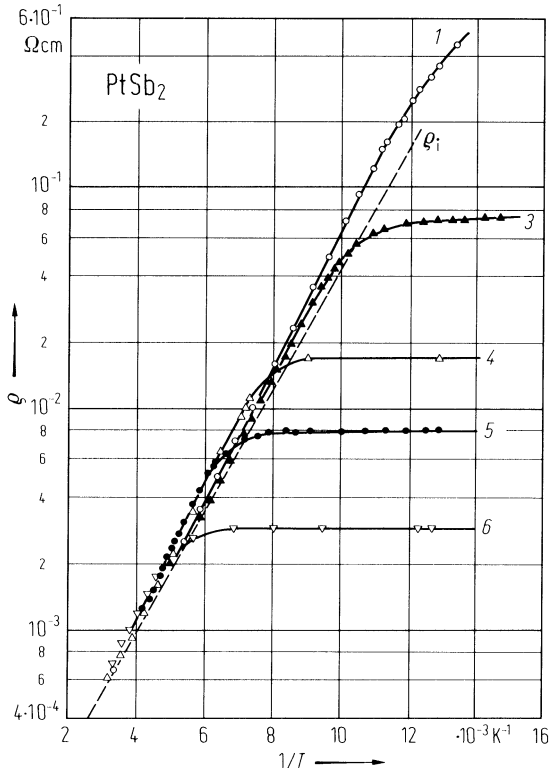

Fig. 4.

$PtSb_2$. Electrical conductivity vs. reciprocal temperature [76A]. The specimens were fragments of a Te-doped single crystal with a Te concentration close to the concentration of residual acceptor impurities in "undoped n-type $PtSb_2$". The donor (Te) concentration was approximately constant ($n_d = 4 \cdot 10^{16}$ cm^{-3}) along the ingot and only the acceptor concentration varied. The samples were cut from the n-type part at right angles to the growth direction [1 1 0]. The sample numbers increase with the degree of compensation (as estimated from R_H in the depletion region). $n_d - n_a$ in 10^{16} cm^{-3}: *1*: 3.2, *2*: 1.9, *3*: 1.4, *4*: 1.2, *5*: 1.0, *6*: 0.7, *7* : 0.3.

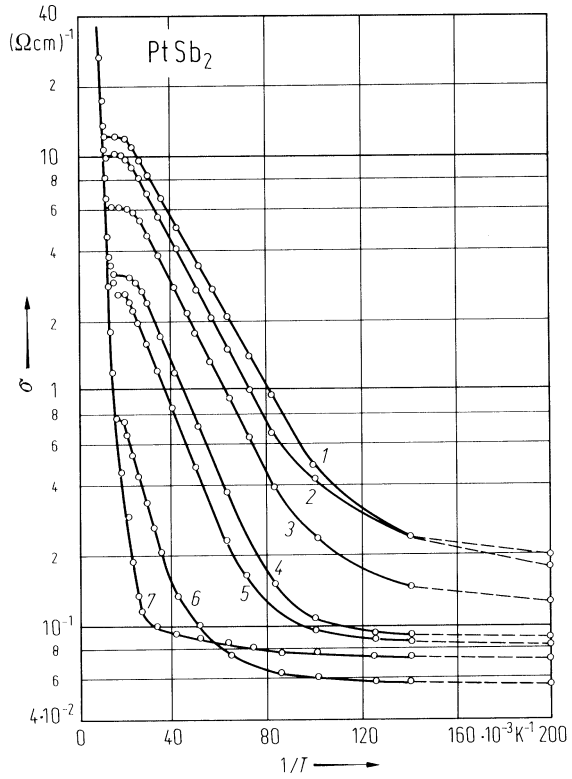

Fig. 5.

$PtSb_2$. Electrical conductivity and Hall coefficient vs. reciprocal temperature for a p-type single crystal [73A]. The energy gap is derived from $A = R_H T^{3/2}(m_n m_p/m_0^2)^{3/4}((1+b)/(1-b))$, where the density of states masses $m_{n,p} = n_{C,V}^{2/3} \cdot m_\parallel^{1/3} \cdot m_\perp^{2/3}$, with $n_{C,V}$ = number of energy ellipsoids, $m_\parallel$ and $m_\perp$ = longitudinal and transverse effective masses, respectively. A in $cm^3\ K^{3/2}\ As^{-1}$.

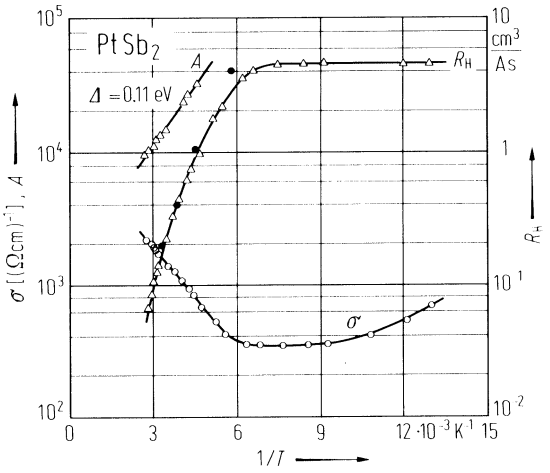

Fig. 6.

$PtSb_2$. Absolute values of the Hall coefficient vs. reciprocal temperature of single crystals [65D].

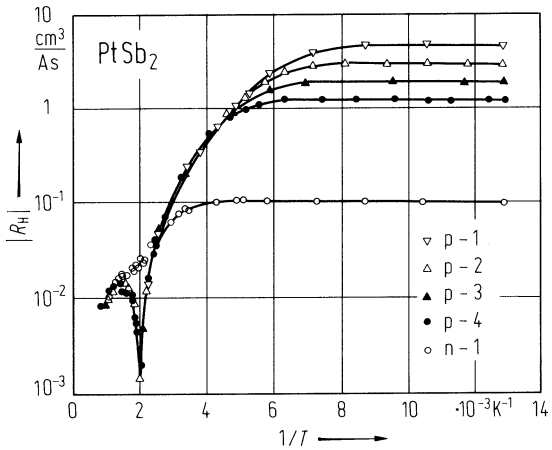

Fig. 7.

$PtSb_2$. Hall coefficients vs. reciprocal temperature for n-type samples [68R]. Extrinsic carrier concentrations $N_{extr.} = n - p = 1/eR_H$ (77K); *1*: $5.68 \cdot 10^{15}$ cm^{-3}, *3*: $5.00 \cdot 10^{16}$ cm^{-3}, *4*: $3.30 \cdot 10^{17}$ cm^{-3}, *5*: $9.93 \cdot 10^{17}$ cm^{-3}, *6*: $5.48 \cdot 10^{18}$ cm^{-3}.

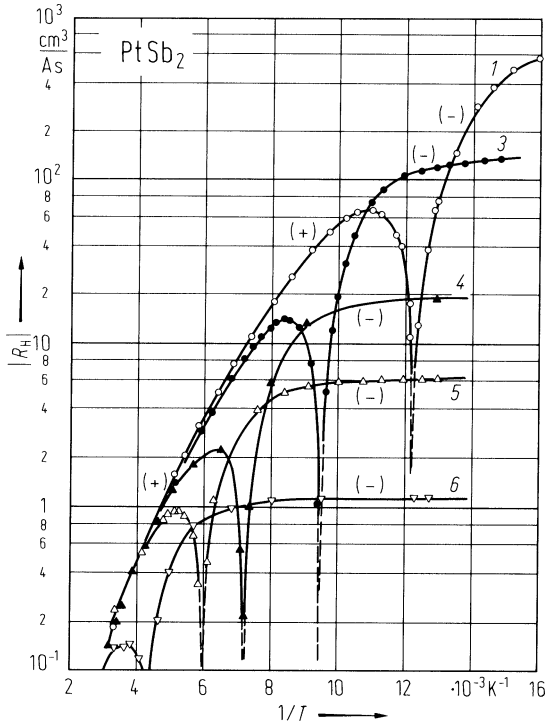

Fig. 8.

$PtSb_2$. Hall coefficient and resistivity vs. reciprocal temperature in the mixed-conduction range for an n-type sample of low impurity contents [68R]. 2N: $N_{extr.} = n - p \approx 2.4 \cdot 10^{16}$ cm^{-3}, $\mu_H(77K) = 3140$ cm^2/Vs; 2P: $P_{extr.} = p - n \approx 6.06 \cdot 10^{16}$ cm^{-3}, $\mu_H(77K) = 5840$ cm^2/Vs.

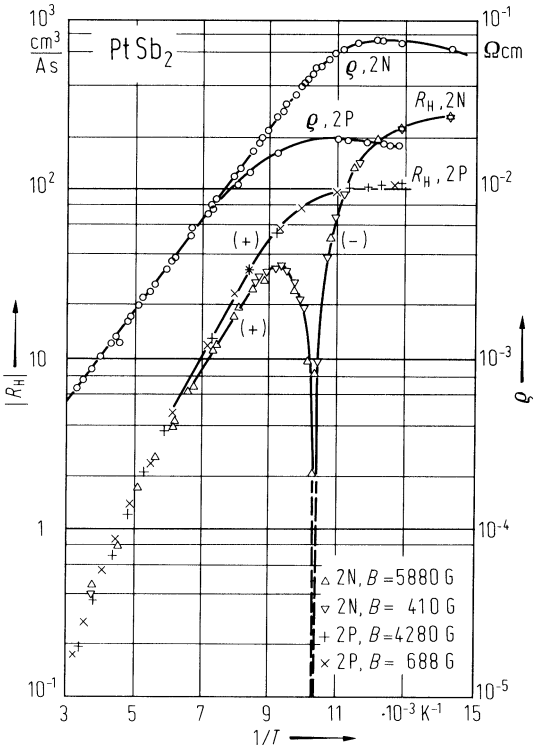

Fig. 9.

$PtSb_2$. Seebeck coefficient vs. temperature [65D]. All samples were single crystals. See Fig. 6. Above ≈ 1000 K the Seebeck coefficient of sample p–3 is negative (≈ –1 μV/K).

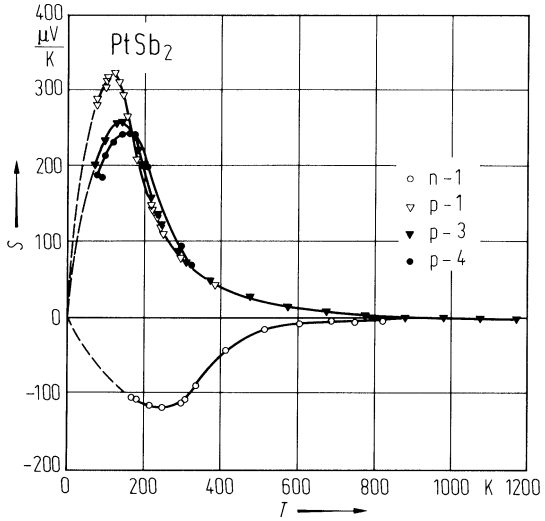

Fig. 10.

$PtSb_2$. Seebeck coefficient vs. reciprocal temperature in the intrinsic region. Circles: Te doped single crystal with $n_d - n_a \approx 10^{17}$ cm^{-3}, $n_a/n_d \approx 0.8$ and $(-eR_H)^{-1} = 6.6 \cdot 10^{16}$ cm^{-3} [83D]. Triangles: Sample p–3 of [65D]; compare Fig. 6.

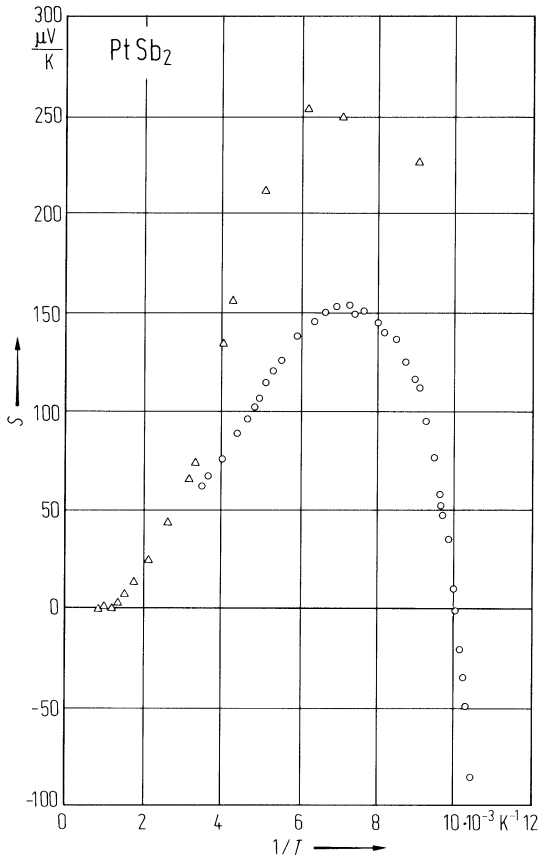

Fig. 11.

$PtSb_2$. Mobilities of electrons and holes and mobility ratio $b = \mu_n/\mu_p$ vs. temperature in the intrinsic region; b derived from $S(T)$ [73A]. $A = \mu_p(m_p/m_0)^{5/2}$ (open circles) and $\mu_n(m_n/m_0)^{5/2}$ (full circles) varies as $\propto T^{-1.3}$.

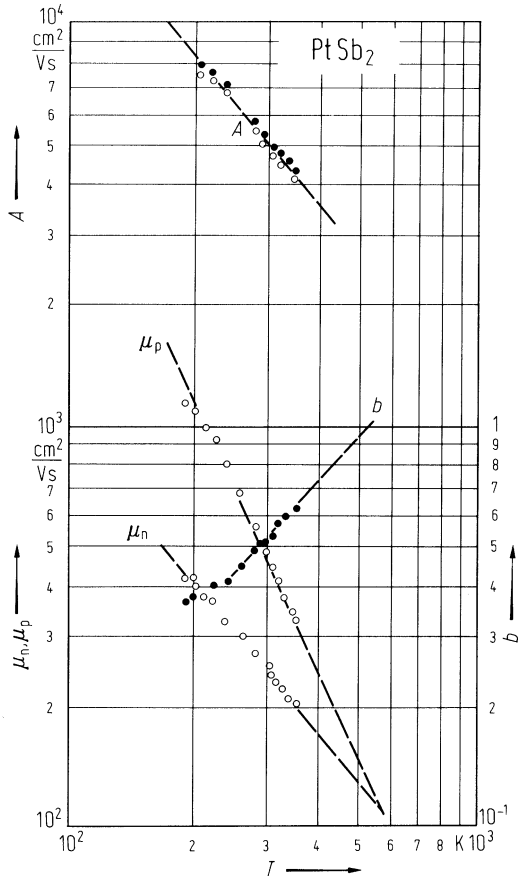

Fig. 12.

$PtSb_2$. Electron and hole mobilities vs. temperature [68R]. The broken lines represent values calculated for the intrinsic range: $\mu_p = 4.15 \cdot 10^6\ T^{-3/2}\ e^{+12.6K/T} \approx 6.55 \cdot 10^6\ T^{-1.57}$. $\mu_n = b\mu_p = 2.07 \cdot 10^6\ T^{-3/2}\ e^{+12.6K/T}$ (T in K), obtained from experimental data of Hall effect and resistivity. 2P, 2N: sample numbers.

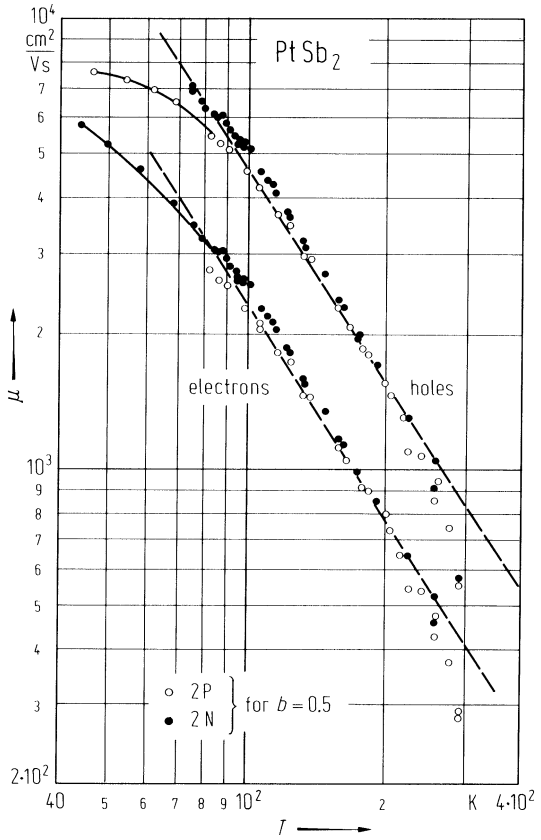

Fig. 13.

$PtSb_2$. Hall mobility vs. temperature in a doubly-logarithmic scale [76A]. Sample numbers as in Fig. 4. At low temperatures the slopes are considerably steeper than for compensated semiconductors when electrons are scattered by ionized impurities i.e. $R\sigma$ ceases to represent the mobility at $T < 20$ K [76A].

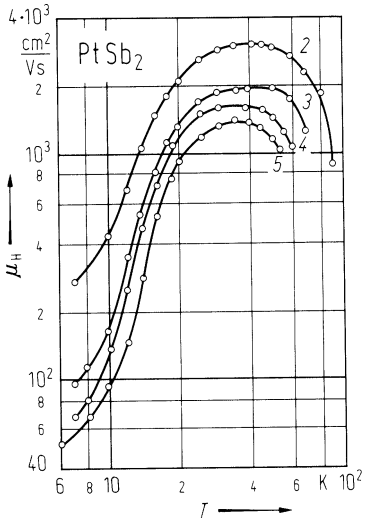

Fig. 14.

$PtSb_2$. $n_iT^{-3/2}$ vs. reciprocal temperature [68R]. For samples 2P and 2N the intrinsic carrier concentration was calculated from $\sigma(T)$, $R_H(T)$ using the relations $n_i^2 = np$ and $n - p = N_{extr.} = (eR_H)^{-1}$ at 77 K, and assuming $b = \mu_n/\mu_p = 0.50$. For samples 1, 3...6 n_i was calculated at T where $R_H = 0$, using $nb^2 = p = n - N_{extr.}$ as well as at the temperature at which R_H reaches a maximum, using $nb = p = n - N_{extr.}$. The mobility ratio b was calculated at the positive maximum of R_H for each n-type sample using the relation $R_H^{max}/R_H^{extr} = (b-1)^2/4b$. The broken line represents $n_iT^{-3/2} = 4.84 \cdot 10^{15}\, A\, e^{-Eg(0)/2kT}$ [$cm^{-3}K^{-3/2}$], where $E_g(0) = 0.110$ eV and $A = (m_n m_p/m_0^2)^{3/4}\, e^{-\beta/2k} = 2\ 72$ ($m_{n,p}$: density of states masses), β: temperature coefficient of the band gap ($E_g = E_g(0) + \beta T$).

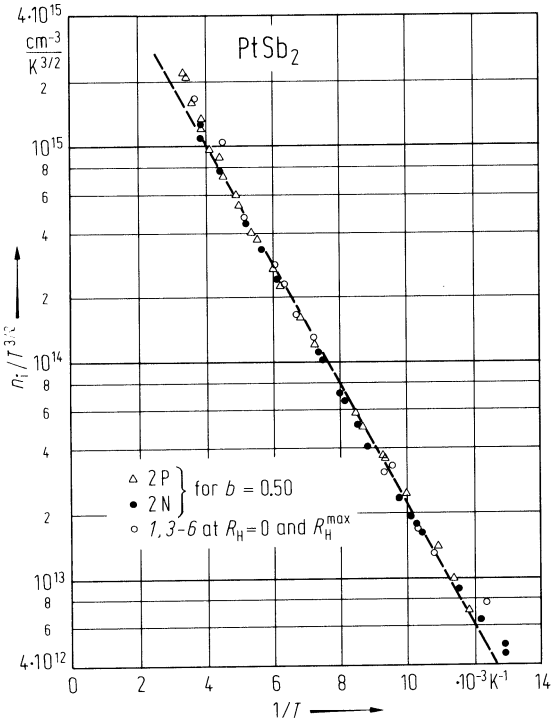

Fig. 15.

$PtSb_2$. Intrinsic carrier concentration vs. reciprocal temperature [73A]. *1*: $n_i T^{-3/2}$ of [73A] calculated from Hall effect and Nernst-Ettingsbausen effect, *2*: $n_i T^{-3/2}$ data taken from [68R]. $C = n_i T^{-3/2} (m_n m_p / m_0^2)^{-3/4}$.

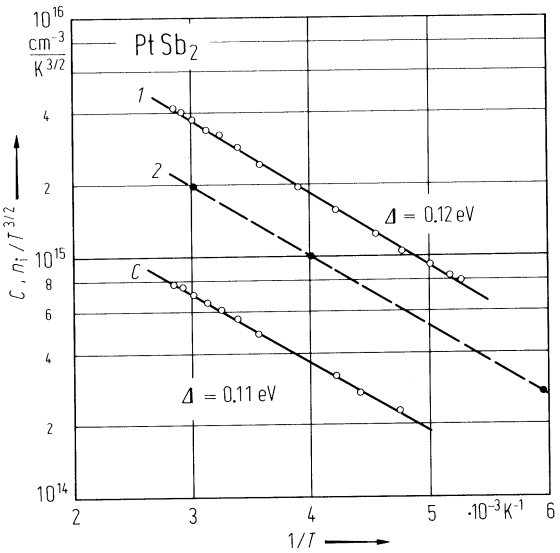

Fig. 16.

$PtSb_2$. Transverse and longitudinal magnetoresistance vs. magnetic field strength [72D]. Monocrystalline p-type sample of low carrier concentration; R_H = 150 cm^3/As, ρ = 0.169 Ωcm, μ_H = 890 cm^2/Vs at 4.2 K.

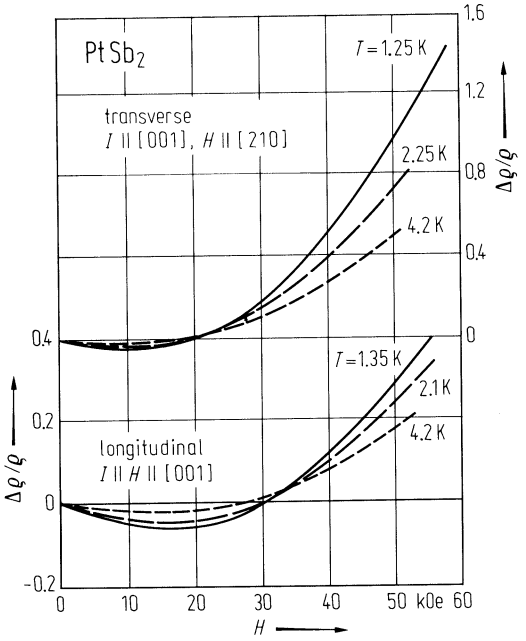

Fig. 17.

$PtSb_2$. Transverse and longitudinal magnetoresistance vs. magnetic field strength [72D]. Mono-crystalline p-type samples with moderate to high carrier concentrations. *2*: Sn-doped, *3,5,6*: Rh-doped.

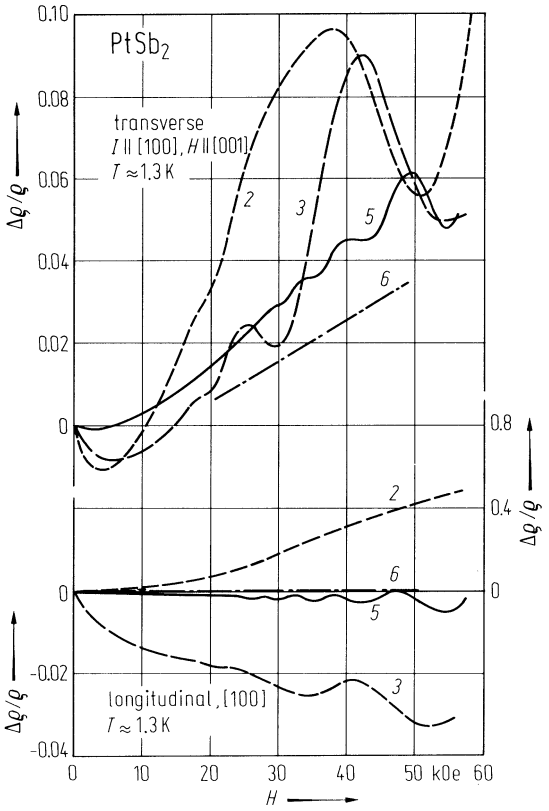

Fig. 18.

$PtSb_2$. Oscillatory part of the longitudinal magnetoconductivity $\Delta\sigma/\sigma$ vs. reciprocal magnetic field [72D]. Longitudinal effect parallel to [100]. Rh-doped p-type single crystal with R_H(4.2 K) = 1.87 cm^3/As, ρ(4.2 K) = $9.14 \cdot 10^{-4}$ Ωcm.

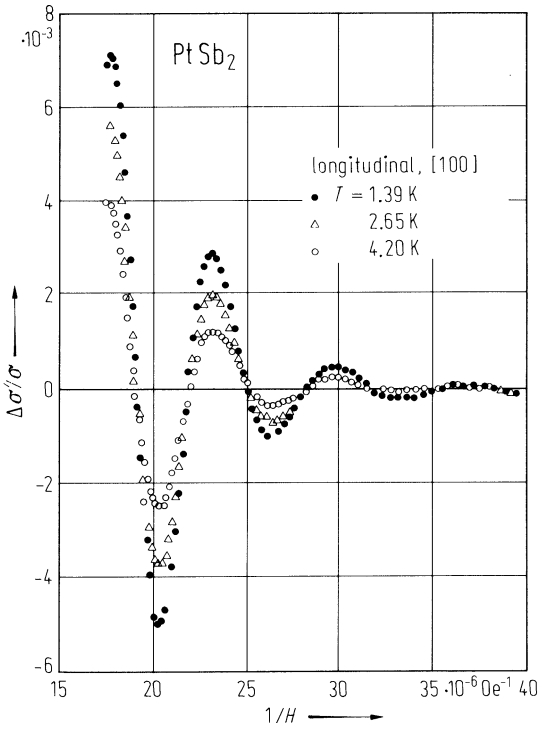

Fig. 19.

$PtSb_2$. Oscillatory part of the transverse magnetoresistance $\Delta\rho'/\rho$ and Hall coefficient $\Delta R'/R$ vs. reciprocal magnetic field strength [72D]. For sample data, see Fig.18.

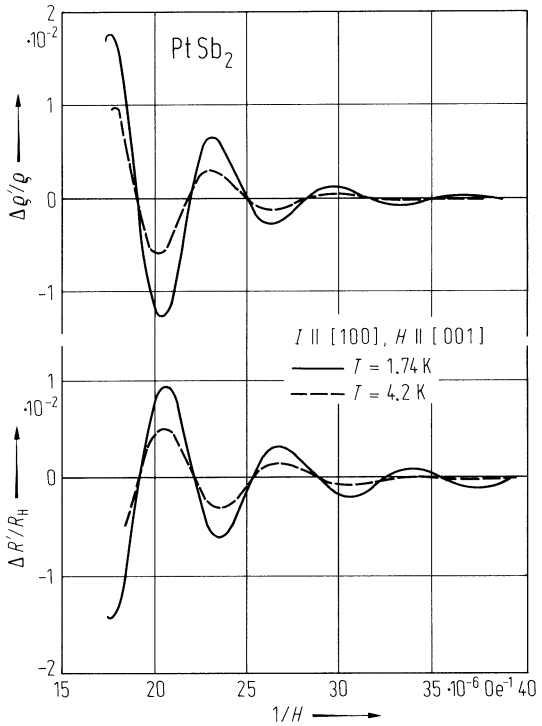

Fig. 20.

$PtSb_2$. Resistance ratio R_p/R_0 vs. hydrostatic pressure [65D]. (1 t/cm^2 = 9.807·10^7 Pa). Triangles and circles: n-type crystal n–1 and p-type crystal p–4, respectively, measured at 195 K (full symbols) and 300 K (open symbols).

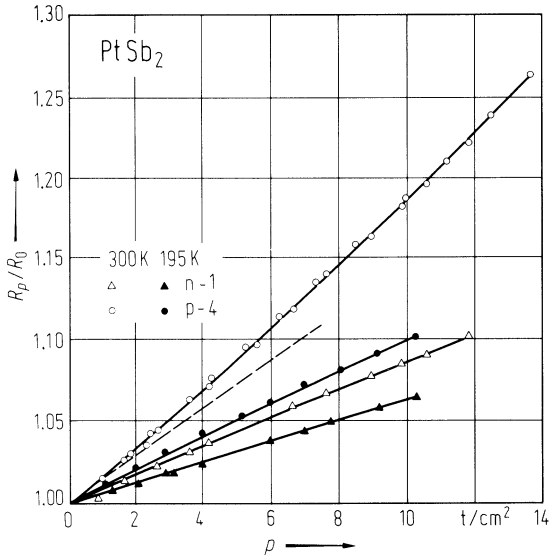

Fig. 21.

$PtSb_2$. Piezoresistance coefficients vs. temperature for various samples (see Fig. 6) [65D].

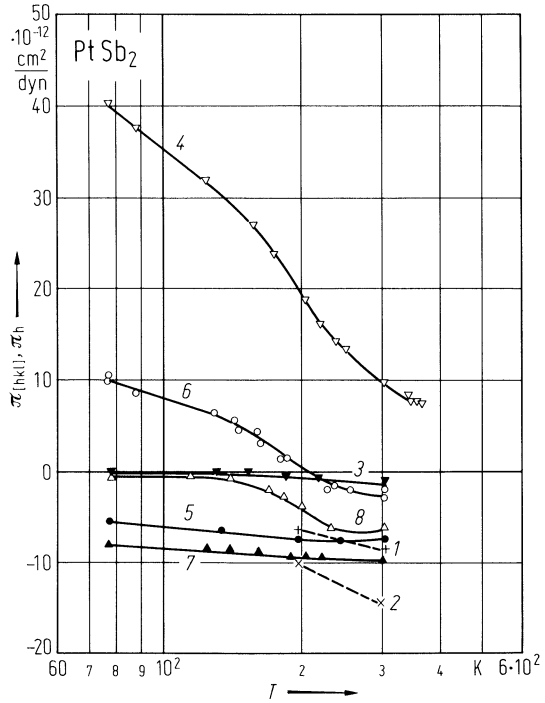

Fig. 22

$PtSb_2$. Thermal conductivity vs. temperature (a) and electrical resistivity vs. temperature (b), both in doubly-logarithmic scale, measured on single crystals of unknown orientation. The resistivity curves serve to characterize the different samples [82K].